Electronic Supplementary Material (ESI) for Journal of Materials Chemistry C.

Supporting Information

Aligned Chromophores in a host-guest MOF Crystal for Switchable Polarized Nonlinear Optical Response

Lin Zhang, Hongjun Li, Yu Yang, Deren Yang, Yuanjing Cui* and Guodong Qian*

State Key Laboratory of Silicon Materials, Cyrus Tang Center for Sensor Materials and
Applications, School of Materials Science and
Engineering, Zhejiang University, Hangzhou 310027, China.
Email: cuiyj@zju.edu.cn, gdqian@zju.edu.cn

1. Experimental Section

Material characterization.

The UV-Vis absorbance spectra of liquid samples were obtained on an UV-2600 UV-Vis spectrophotometer (Shimadzu, Japan). A Micromeritics ASAP 2020 surface area analyzer were used to measure N_2 adsorption isotherms. To remove the solvents in MOF channels, the ZJU-24-Eu and ZJU-24-Eu⊃DSM crystals were exchanged with ethanol at least 10 times in three days, filtered and evacuated at 373 K for 24 h until the outgas rate was 3 μmHg min^{-1} prior to measurements. Fourier transform infrared (FTIR) spectra were recorded on a Thermo Fisher Nicolet iS10 spectrometer by using KBr pallets. The pallets were fabricated by mixing the sample and KBr. The mixture was then grinded and compressed under a pressure of 400 kgf cm^{-2} to form the transparent pallets. The ^{1}H nuclear magnetic resonance (NMR) spectrum was obtained from a Bruker Advance DMX500 spectrometer. The ZJU-24-Eu⊃DSM (5 mg) was dissolved in DMSO-d_6 with 20 μL DCl.

The morphology of MOF single crystals was investigated through using a field emission scanning electron microscopy (FE-SEM, Hitachi S4800). The optical images of MOF single crystals were captured by an Olympus IX 71 inverted fluorescent microscope under the irradiation of halogen lamps, mercury lamps or femtosecond (fs) laser. Powder X-ray diffraction (PXRD) data of MOF samples were obtained from a PANalytical X'Pert Pro X-ray diffractometer employing a Cu Kα (λ= 1.542 Å) beam with 2θ ranging from 3° to 45° at room temperature. The simulation of crystal channel and morphology is completed by the software Materials Studio. The UV-Vis absorbance spectra of solid samples were recorded on a TU1901 spectrometer equipped with an integral sphere. The solid samples were added into $BaSO_4$ before tests. Excitation and emission spectra were measured by a Hitachi F-4600 spectrometer. The quantum yield was recorded on an Edinburgh Instrument F920 spectrometer. A picosecond (ps) laser of 405 nm was used as excitation source for measuring lifetime of ZJU-24-Eu⊃DSM microcrystalline powder.

NLO switching test

The sample were put on the microscope stage in Fig. S16. One isolated crystal was chosen to be excited by a polarized fs laser (1064 nm). During the test, the sample and stage were not moved and touched at all. A half-wave plate was rotated to change the polarized direction of the incident laser, and the corresponding signals were recorded by a high-resolution fiber optic spectrometer (PG2000-Pro, Ideaoptics Instruments).

SHG evaluation

Based on the modified Kurtz powder technique, we further compared the SHG intensity of ZJU-24-Eu⊃DSM to that of ZJU-24-Eu.[1, 2] The as-prepared ZJU-24-Eu and ZJU-24-Eu⊃DSM crystals were sieved carefully into microcrystalline powders with a wide size distribution range from 25 to 61 μm. To exclude potential uncertainties due to the preferred orientation and distinct particle sizes, each powder sample was measured for 4 times and the sample would be refreshed after every test. Both two microcrystalline powder samples were excited by a beam of 1064 nm laser, and the SHG signals were collected by the fiber optic spectrometer. The corresponding intensities of the as-collected signals are shown in Fig. S19 below.

Determination of two-photon absorption section

Based on a widely-accepted fluorescence ratio method, the two-photon absorption section of ZJU-24-Eu⊃DSM was obtained by using R6G ethanol solution (10^{-4} M) as a reference sample.[3, 4] The formula $\eta_z\sigma_z = (I_z/I_r)(\rho_r/\rho_z)\eta_r\sigma_r$ was used to estimate the two-photon absorption cross section of ZJU-24-Eu⊃DSM, where η is the quantum yield, σ is the two-photon absorption cross section, and ρ is the molar concentration. I_z and I_r were the measured two-photon excited fluorescence (2PEF) intensities of ZJU-24-Eu⊃DSM microcrystalline powders and R6G solution, respectively. These two parameters could be obtained based on the experimental devices in Fig. S16, where ZJU-24-Eu⊃DSM crystal and the reference R6G solution were excited by a beam of fs laser (1060 nm, 10kHz) (Fig. S20). The use of higher repetition frequency (10 kHz) is due to that R6G solution emit extremely weak 2PEF signal when pumped by 1060 nm at 2 kHz. All the other experimental conditions are kept the same. The σ_r of the standard R6G sample is reported to be 9.9 GM at 1060 nm and the η_r of R6G 10^{-4} M ethanol solution is ~ 89.5%.[5, 6] The molar concentration of DSM in ZJU-24-Eu⊃DSM could be calculated by the formula: $\rho_z = nR/(N_AV)$, where R could be obtained from the formula of ZJU-24-Eu⊃DSM $[(DSM)_REu(C_{39}H_{24}NO_6)]$ and n is the number of secondary construction units in a unit cell of ZJU-24-Eu. According to the as-obtained dye content (mass fraction, 2.29 wt%), the value of R is approximately 0.048. Each unit cell in the structure of ZJU-24-Eu has four secondary construction units to load DSM molecules, thus the value of n is 4. Based on the unit cell volume V = 4010.24 Å^3 and $N_A = 6.02 \times 10^{23}$ mol^{-1}, ρ_z is calculated to be 0.080 M. Therefore, the value of η_z is approximately 8.55 GM.

2. Supplementary Figures

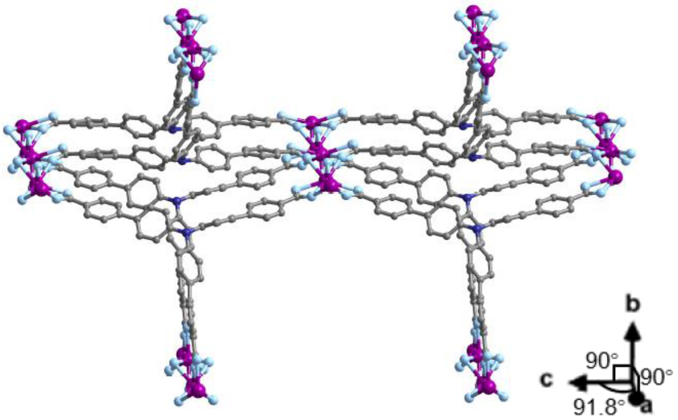

Fig. S1. Every ligand in the structure of ZJU-24-Eu has the same coordination environment and its phenyl arms have different orientations. Eu: purple; O: light blue; N: dark blue; C: grey. All hydrogen atoms are omitted.

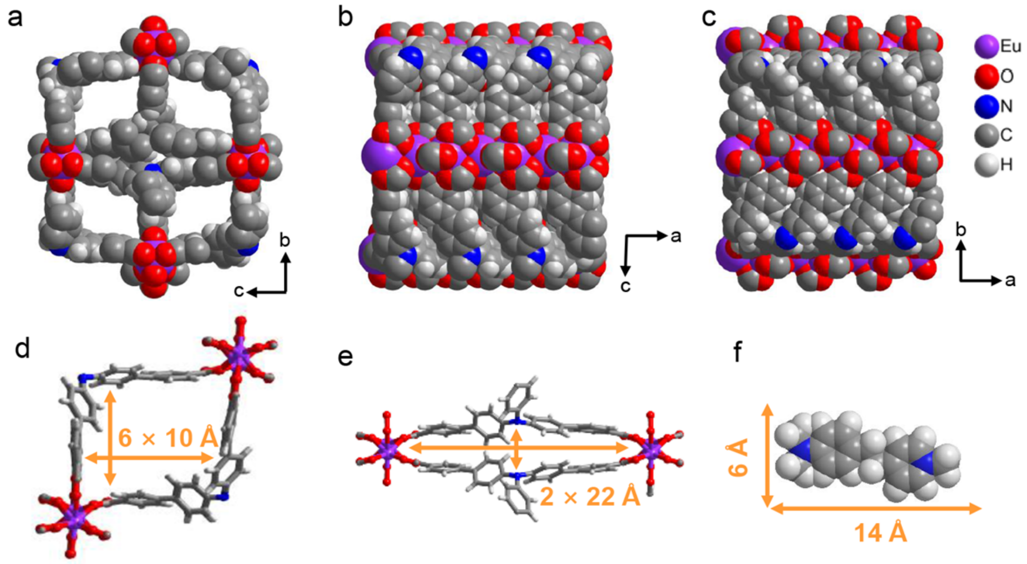

Fig. S2. The space filling model structure of ZJU-24-Eu viewed along (a) *a*-axis, (b) *b*-axis, and (c) *c*-axis, which show clearly 1D channels along *a*-axis. The 1D channels have two different pore sizes of (d) 6 × 10 Å^2 and (e) 2 × 22 Å^2. (f) The space filling model structure of the DSM dye.

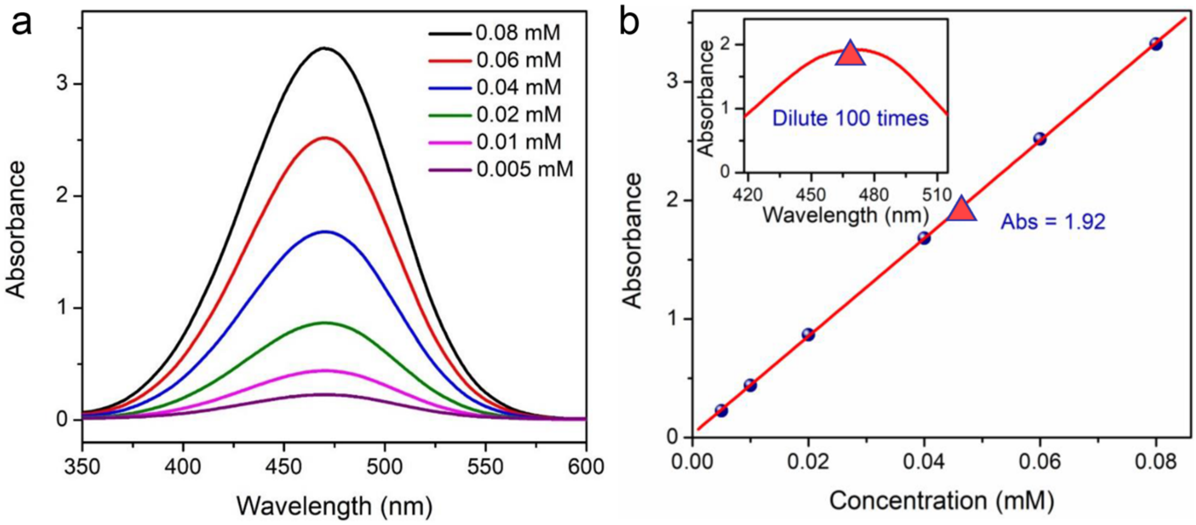

Fig. S3. (a) The absorption spectra of DSM-dissolved DMF solution of different concentrations. (b) The linear relationship between DSM contents and absorbance peaks (λ_{max} = 470 nm). Inset: absorbance spectrum of the residual DSM solution after preparing ZJU-24-Eu⊃DSM. The DSM concentration in the obtained MOF⊃dye crystals was determined to be about 2.29 wt%.

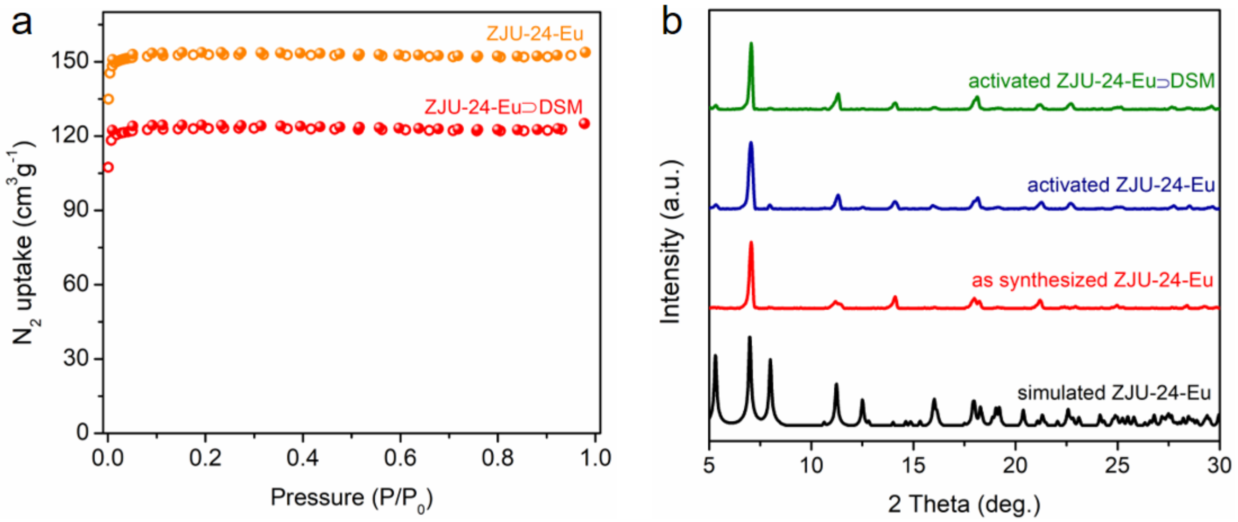

Fig. S4. (a) N_2 adsorption isotherms at 77 K of ZJU-24-Eu and ZJU-24-Eu⊃DSM. (b) The PXRD patterns of the activated ZJU-24-Eu and ZJU-24-Eu⊃DSM, showing that these materials keep the same structure after activation.

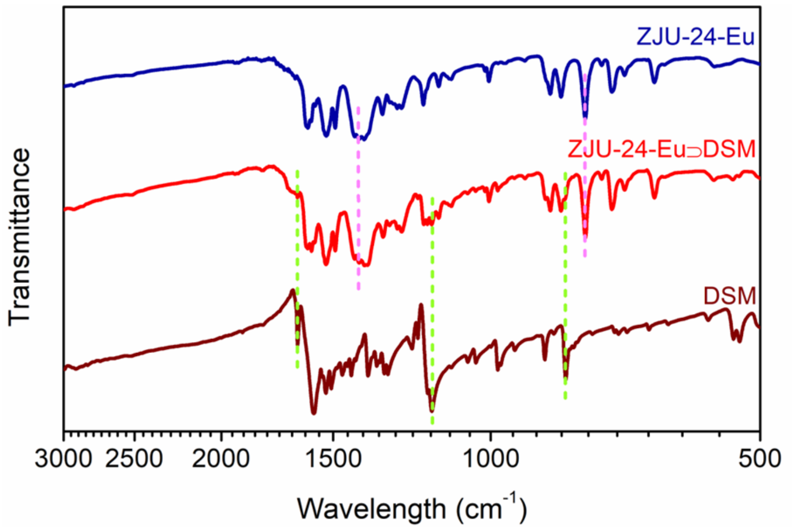

Fig. 5. FTIR spectra of ZJU-24-Eu, DSM and ZJU-24-Eu⊃DSM.

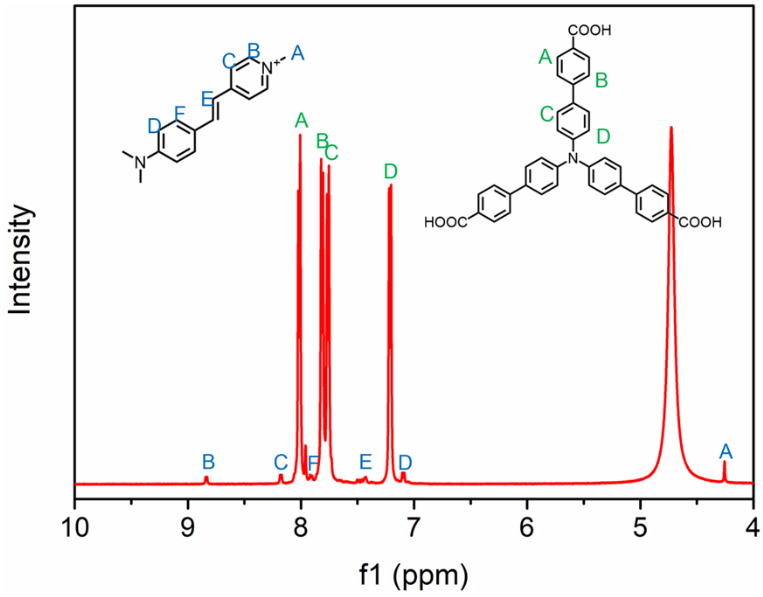

Fig. 6. The ^{1}H NMR (500MHz) spectrum of ZJU-24-Eu⊃DSM dissolved in DMSO-d_6 and DCl.

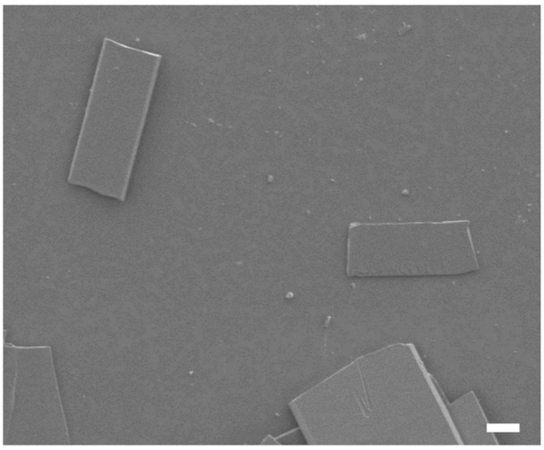

Fig. S7. The SEM image of ZJU-24-Eu⊃DSM microplates. Scale bar, 20 μm.

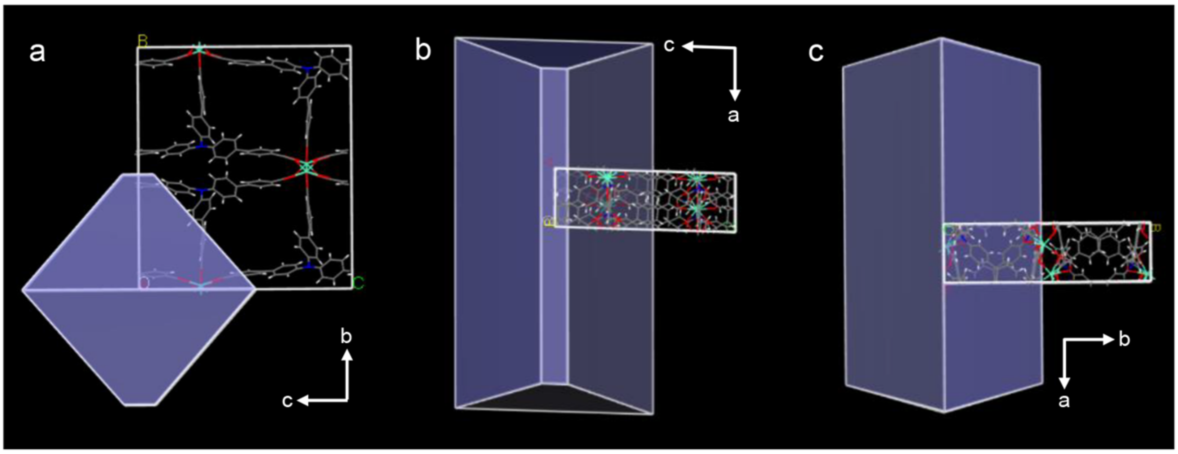

Fig. S8. The simulated crystal morphology of ZJU-24-Eu crystal along (a) *a*-axis, (b) *b*-axis and (c) *c*-axis, which is obtained by using the Bravais-Friedel-Donnay-Harker method.

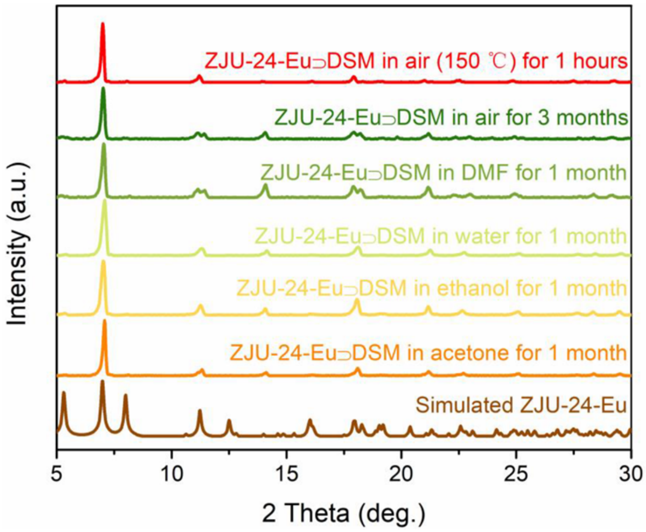

Fig. S9. PXRD patterns of ZJU-24-Eu⊃DSM in the air and common solvents such as acetone, ethanol, water and DMF, and after heat treatment, showing great stability.

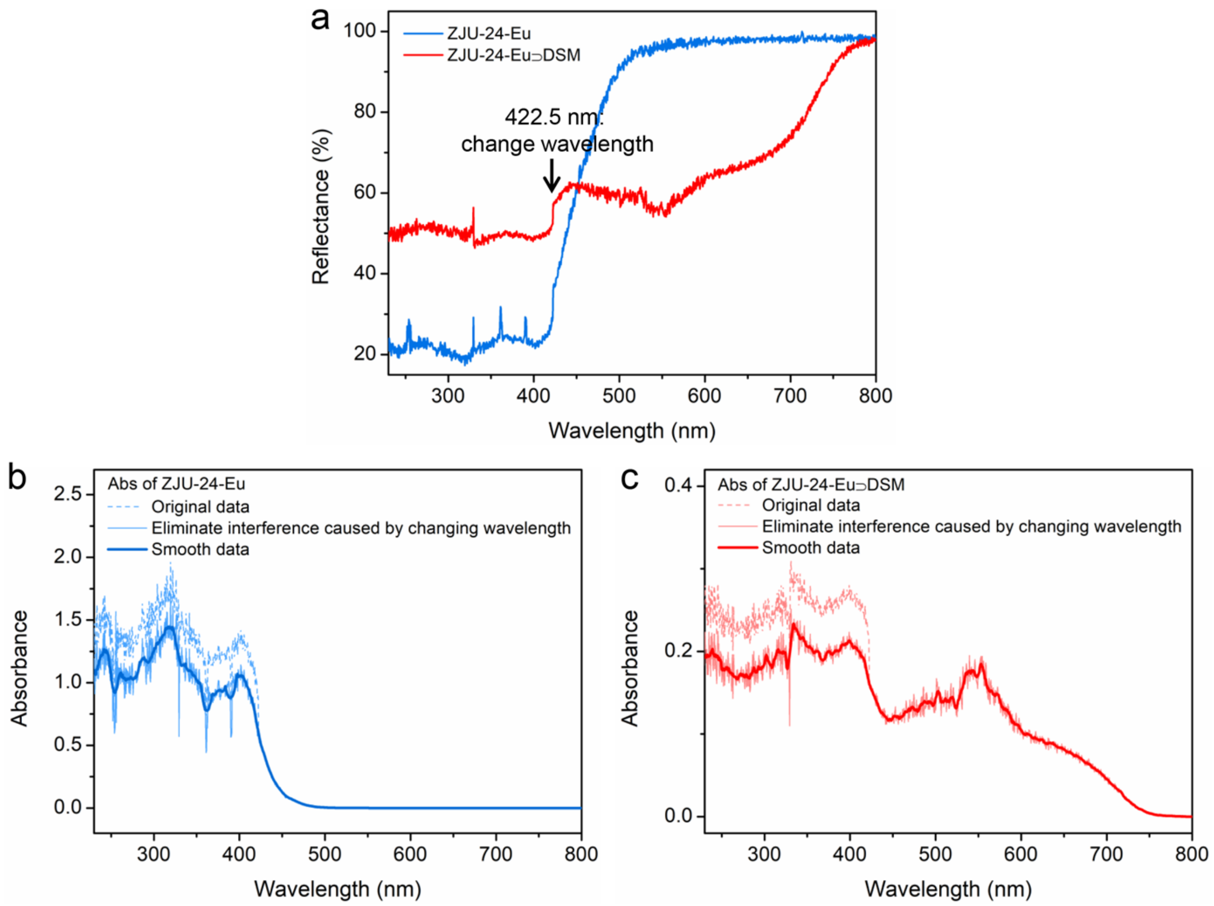

Fig. S10. (a) The diffuse reflectance spectra of ZJU-24-Eu and ZJU-24-Eu⊃DSM microcrystalline powders. The absorption spectra of (b) ZJU-24-Eu and (c) ZJU-24-Eu⊃DSM microcrystalline powders which are transformed from the above diffuse reflectance spectra.

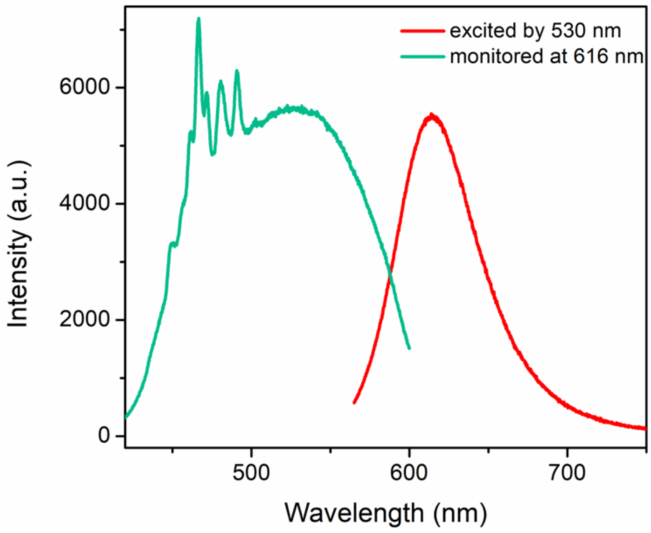

Fig. S11. The excitation and emission spectra of ZJU-24-Eu⊃DSM microcrystalline powders.

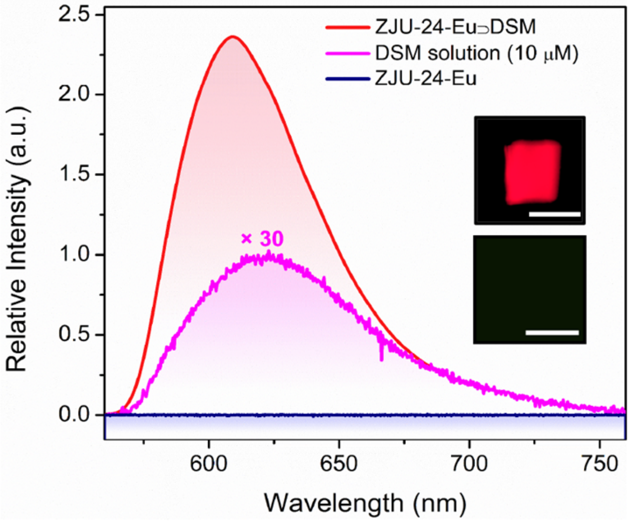

Fig. S12. Emission spectra (λ_{Ex} = 532 nm) of DSM solution (10 μM), ZJU-24-Eu and ZJU-24-Eu⊃DSM. Insets: the optical micrographs of ZJU-24-Eu (bottom) and ZJU-24-Eu⊃DSM single crystal (top) under the excitation of 532 nm. Scale bar, 20 μm.

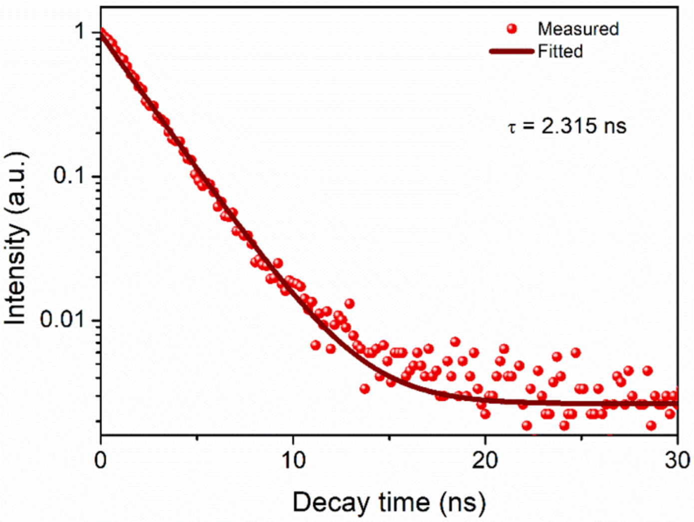

Fig. S13. The lifetime of ZJU-24-Eu⊃DSM.

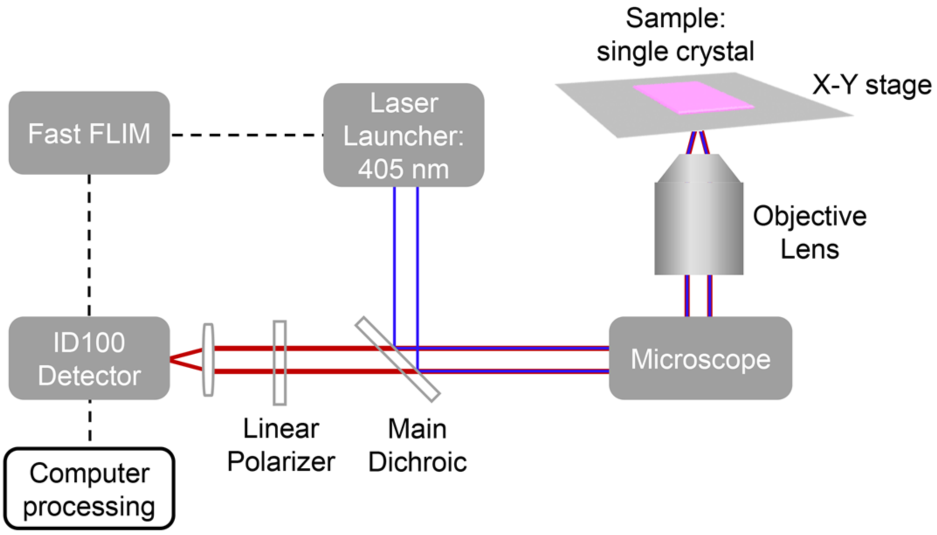

Fig. S14. Schematic diagram of the experimental device for polarization fluorescence imaging conducted by recording the number of photons. The excitation polarization direction is kept parallel with the longitudinal direction of a single ZJU-24-Eu⊃DSM crystal, and a linear polarizer is set before the single photon counting detector ID-100 to control the received photon numbers from the excited crystal. On account of the poor fluorescence of ZJU-24-Eu, almost all the photon numbers from the ZJU-24-Eu⊃DSM crystal were thought to come from DSM molecules. The Fast FLIM module can be employed to record the lifetime of the sample.

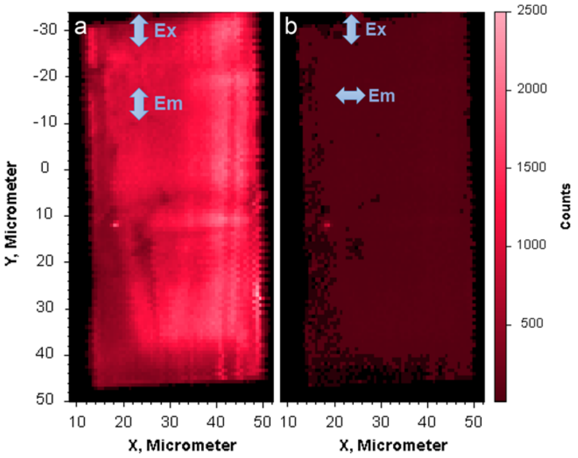

Fig. S15. Polarization fluorescence images of a single ZJU-24-Eu⊃DSM crystal when the emission polarization direction is (a) parallel or (b) perpendicular to the crystal longitudinal direction.

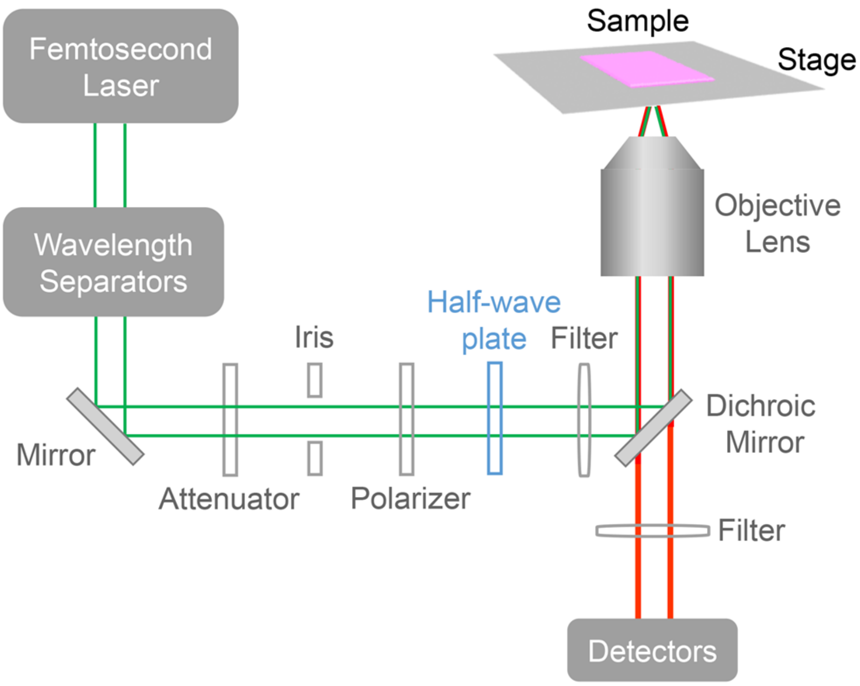

Fig. S16. Experimental setup for measuring NLO and lasing signals. The polarizer is used to purify the pump laser source. The polarization direction of the excitation light is altered by rotating the half-wave plate, which is kept either parallel or perpendicular to the longitudinal direction of crystal. The half-wave plate is only used for the excitation polarization dependence measurements, and it can be dismounted when the tests are unrelated to polarization measurements. Detectors include the CCD camera and fiber optic spectrometer.

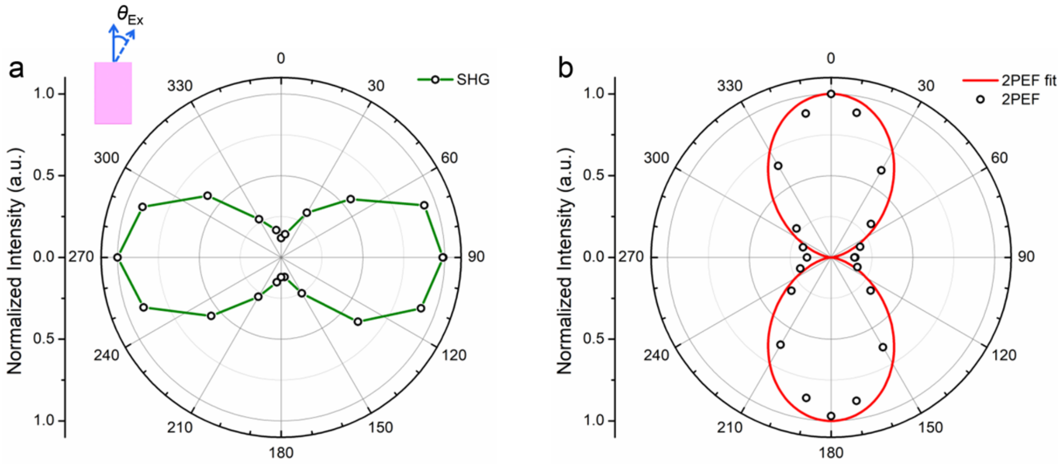

Fig. S17. Polar plots of (a) SHG and (b) 2PEF intensities from a single ZJU-24-Eu⊃DSM crystal as the function of θ_{Ex}. Inset: the schematic illustration of the measurement geometry for a single crystal. The red line represents the $\cos^2\theta$ ($\theta = \theta_{Ex}$) fits for 2PEF response. The SHG response would not be fitted with $\cos^4\theta$ ($\theta = \pi/2 - \theta_{Ex}$) very well because its polarization dependence is not only originating from the MOF, but also affected by the encapsulated dye.

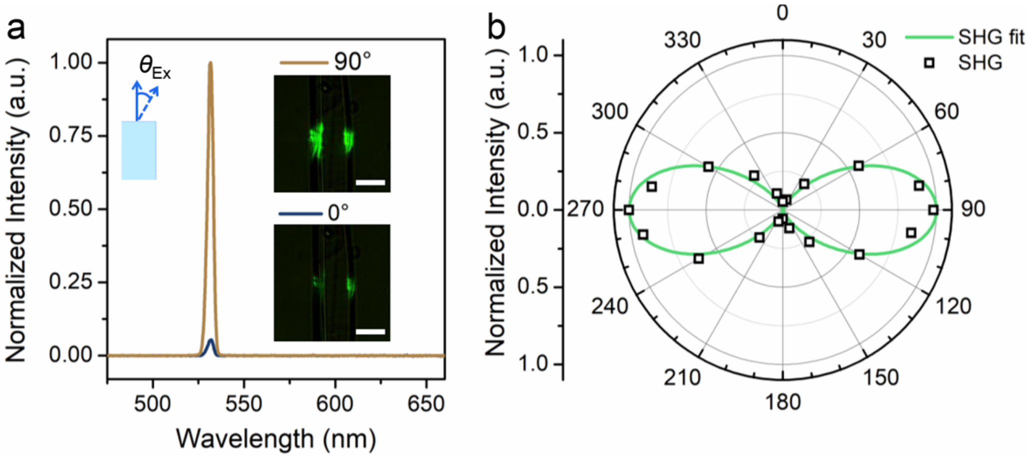

Fig. S18. (a) The SHG spectra of a single ZJU-24-Eu crystal excited under θ_{Ex} = 0° and 90°, respectively. Insets: the schematic illustration of the measurement geometry for a single ZJU-24-Eu crystal (left), and SHG micrographs of the excited ZJU-24-Eu crystal at different θ_{Ex} (right). Scale bar, 25 μm. (b) Polar plot of SHG intensity from ZJU-24-Eu as a function of θ_{Ex}. The green line represents the $\cos^4\theta$ ($\theta = \pi/2 - \theta_{\mathrm{Ex}}$) fits for SHG response.

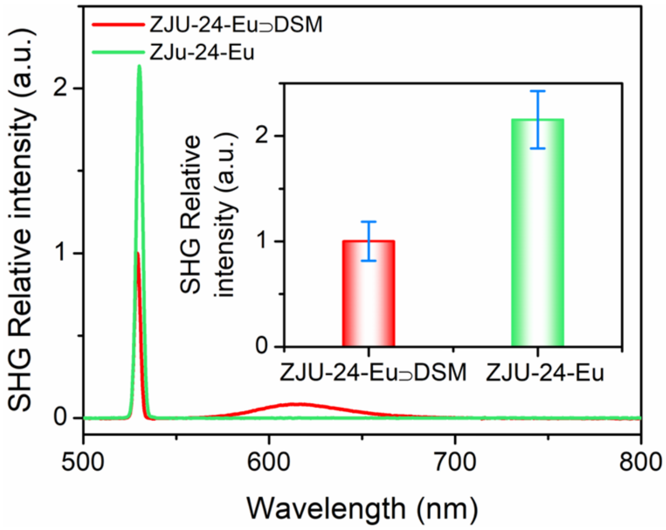

Fig. S19. Two representative spectra of ZJU-24-Eu and ZJU-24-Eu⊃DSM microcrystalline powders, with the particle sizes ranging from 25 to 61 μm. Inset: the comparison of SHG intensity between ZJU-24-Eu and ZJU-24-Eu⊃DSM. The SHG intensity of ZJU-24-Eu microcrystalline powder is about 2.15 times stronger than that of ZJU-24-Eu⊃DSM powder. This phenomenon is most likely due to that dye molecules absorb part of the excitation laser through the two-photon absorption process in the non-centrosymmetric ZJU-24-Eu. It would lead to the competition for excitation light between SHG and two-photon absorption process, resulting in the energy loss of the 1064 nm laser for producing SHG and the decrease of SHG signal intensity in the hybrid ZJU-24-Eu⊃DSM powder.

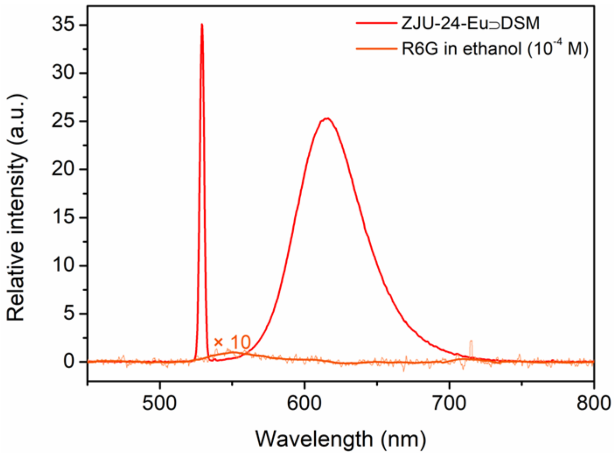

Fig. S20. The two-photon-excited (1060 nm, 10 kHz) luminescence of ZJU-24-Eu⊃DSM and R6G ethanol solution (10^{-4} M).

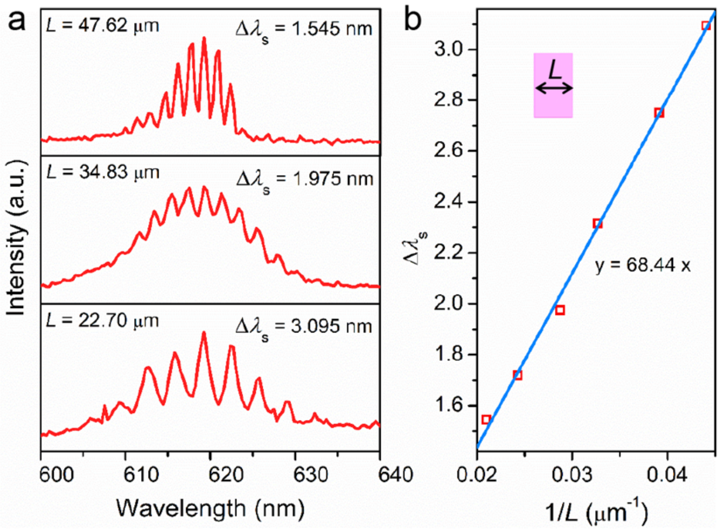

Fig. S21. (a) Lasing spectra of ZJU-24-Eu⊃DSM microplates with different sizes, for confirming the F-P effect. (b) The value of $\Delta\lambda$ with respect to $1/L$ of the ZJU-24-Eu⊃DSM microplate, matching the equation $\Delta\lambda = \lambda^2/2n_gL$. Inset: the feedback path length (L) in a plate-like microcrystal. The n_g derived from the linear relationship between the measured $\Delta\lambda$ and $1/L$ is around 2.81, which is high enough for improving the confinement effect of F-P cavity.

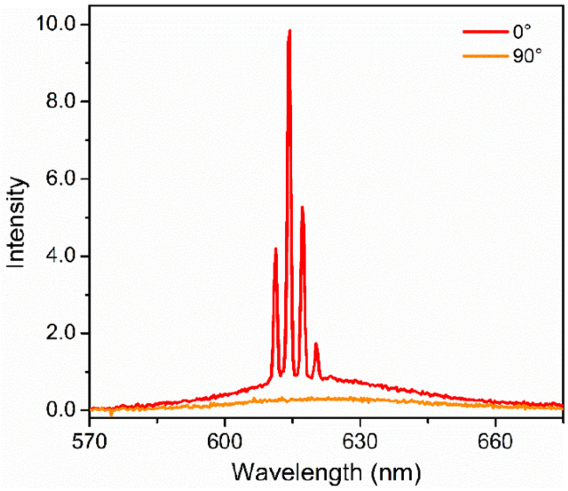

Fig. S22. The TPP lasing intensity of a single ZJU-24-Eu⊃DSM crystal vs. excitation polarization direction. A strong TPP lasing signal with highly-structured spectrum can be observed at $\theta_{\text{Ex}} = 0°$ while turned to a much weaker 2PEF signal at $\theta_{\text{Ex}} = 90°$

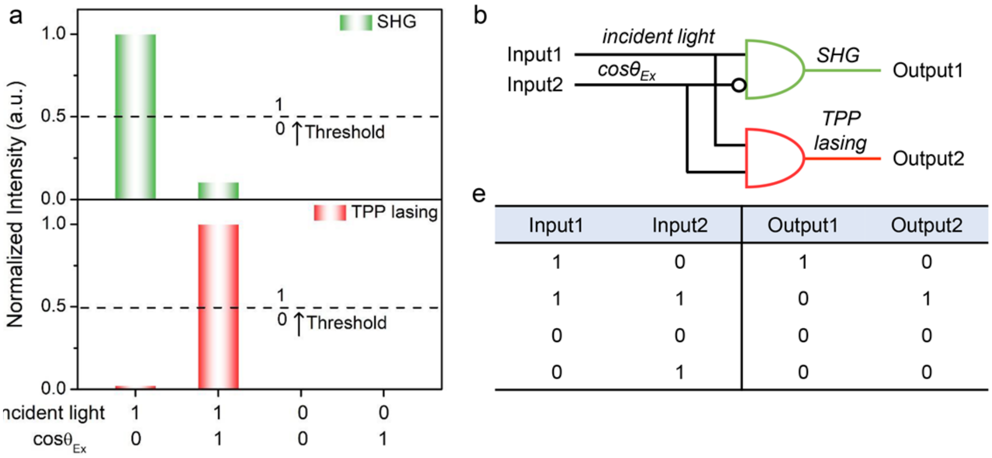

Input1	Input2	Output1	Output2
1	0	1	0
1	1	0	1
0	0	0	0
0	1	0	0

Fig. S23. (a) The normalized intensities of SHG and TPP lasing in the form of bar representation at four possible input states. The output intensity below the presupposed threshold level (0.5) is translated into binary "0", otherwise it will be defined as binary "1". (b) A combinational logic circuit consisting of an INHIBIT and an AND logic gates where the incident light and excitation polarization direction serve as two inputs and the SHG and TPP lasing signals represent as two outputs, which owns potential to be applied into multichannel optical communication. (c) Truth table of the combinational logic circuit.

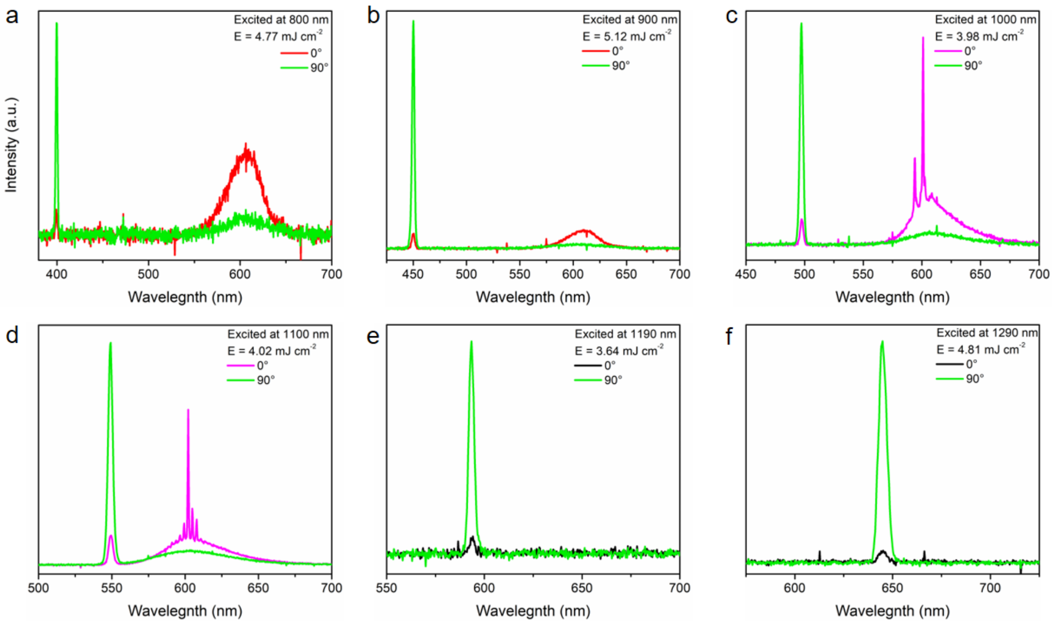

Fig. S24. The NLO properties and the corresponding excitation polarization dependence of ZJU-24-Eu⊃DSM excited at (a) 800, (b) 900, (c) 1000, (d) 1100, (e) 1190 and (f) 1290 nm, respectively. Upon the excitation of 800, 900, 1000 and 1100 nm, ZJU-24-Eu⊃DSM exhibits significant NLO properties including SHG and two-photon response. When the excitation wavelength is increased to 1190 and 1290 nm, ZJU-24-Eu⊃DSM behave SHG responses without the obvious 2PEF signal. All these NLO signals have excitation polarization dependence.

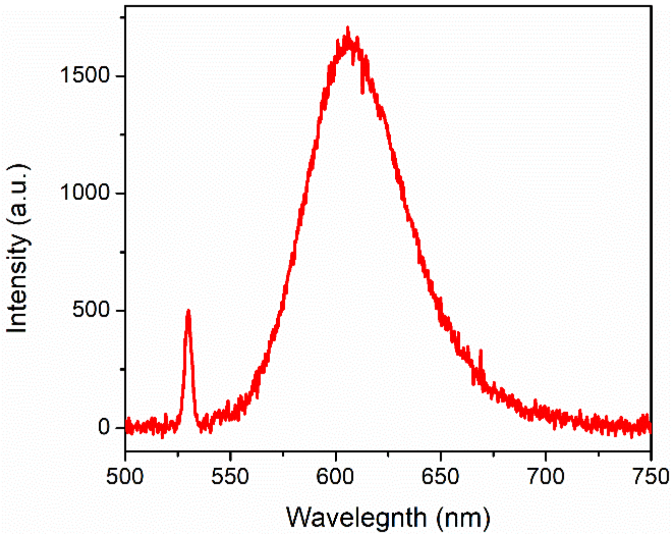

Fig. S25. The spectra (λ_{ex} = 1064 nm) of the ZJU-24-Eu⊃DSM crystal that prepared by immersing ZJU-24-Eu in a DMF solution of low DSM concentration (4 mM), which cannot show lasing performance even if the energy density is as high as 4.65 mJ cm^{-2}.

3. Reference

1 H. Zhang, M. Zhang, S. Pan, X. Dong, Z. Yang, X. Hou, Z. Wang, K. B. Chang and K. R. Poeppelmeier, *J. Am. Chem. Soc.*, 2015, **137**, 8360-8363.
2 S. K. Kurtz and T. T. Perry, *J. Appl. Phys.*, 1968, **39**, 3798-3813.

3 C.-X. Chen, S.-Y. Yin, Z.-W. Wei, Q.-F. Qiu, N.-X. Zhu, Y.-N. Fan, M. Pan and C.-Y. Su, *Angew. Chem. Int. Ed.*, 2019, **58**, 14379-14385.

4 Z. Chen, G. Gallo, V. A. Sawant, T. Zhang, M. Zhu, L. Liang, A. Chanthapally, G. Bolla, H. S. Quah, X. Liu, K. P. Loh, R. E. Dinnebier, Q. H. Xu and J. J. Vittal, *Angew. Chem. Int. Ed.*, 2019, **59**, 833-838.

5 N. S. Makarov, M. Drobizhev and A. Rebane, *Opt. Express*, 2008, **16**, 4029-4047.

6 L. S. Rohwer and J. E. Martin, *J. Lumin.*, 2005, **115**, 77-90.